RSC Advances

PAPER

View Article Online
View Journal | View Issue

Cite this: *RSC Adv.*, 2015, **5**, 43581

Preparation of a ROMP-type imidazolium-functionalized norbornene ionic liquid block copolymer and the electrochemical property for lithium-ion batteries polyelectrolyte membranes†

Juan Wang,[a] Xiaohui He,*[ab] Hongyu Zhu[a] and Defu Chen[c]

Received 19th March 2015
Accepted 7th May 2015

DOI: 10.1039/c5ra04860e

www.rsc.org/advances

Imidazolium-functionalized norbornene ionic liquid block copolymers are synthesized *via* ring-opening metathesis polymerization (ROMP). The solid polyelectrolytes were prepared by blending the copolymers with various contents of lithium bis(trifluoromethanesulphonyl)imide. The effects of the polymerized ionic liquid (PILs) compositions on the properties, morphology, and ionic conductivity of the polyelectrolytes are investigated. The polymer with 50.7 mol% PIL displays a long-range ordered lamellar structure, and its corresponding polyelectrolyte achieves the best ionic conductivity with 7.44×10^{-6} S cm^{-1} at 30 °C and 4.68×10^{-4} S cm^{-1} at 100 °C, respectively. The ionic conductivity is enhanced by 1 order of magnitude compared to the polyelectrolytes with lower polymerized ionic liquid block compositions. In addition, the polyelectrolytes are electrochemically stability up to 4.2 V *versus* Li/Li$^+$, indicating their suitable electrochemical property for lithium-ion battery application.

1. Introduction

Solid polymer electrolytes (SPEs) have been extensively studied for several decades as an alternative for the traditional liquid electrolyte in lithium-ion batteries due to their superior safety and mechanical properties.[1–4] However, the SPEs exhibit fairly low ionic conductivity at room temperature, well below the 10^{-3} S cm^{-1} minimum required for practical battery electrolytes,[5] and thus limits their feasibility for commercial application. So the key challenge is to improve the ionic conductivity of the solid polymer electrolytes.

Polymerized ionic liquids (PILs) display the outstanding performance of ionic liquids such as the unique nonvolatile, non-flammability, large electrochemical window, high ionic conductivity, and the good film-forming of polymers,[6–8] and thus they have been considered as a new type of materials of solid polymer electrolytes. Recently, various PIL electrolytes have been synthesized, such as tetraalkylammonium-type poly(IL)s,[9,10] imidazolium-based poly(IL)s,[11–16] and poly(pyrrolidinium),[6,17] and the corresponding physical and chemical properties, ionic conductivity, and microphase separation have also been characterized. For example, Elabd *et al.*[11,12] synthesized a series of PIL diblock copolymers, and the ionic conductivity is 0.88 mS cm^{-1} at 25 °C. With the similar PIL compositions, the ionic conductivity of the block copolymers increased 2 orders of magnitude compared to the random copolymers, and the block copolymers film can form strong microphase-separated to further increase ionic conductivity. Moreover, Yang[18] synthesized a novel polymeric ionic liquid owning the well thermal and electrochemical stability and high lithium ion conductivity simultaneously. Thus, the PIL electrolytes have been already applied to lithium ion battery.[9,10,13,19]

In this work, a series of imidazolium-functionalized norbornene ionic liquid block copolymers were synthesized *via* ring-opening metathesis polymerization (ROMP) (Scheme 1). We expect that the block copolymers can achieve excellent film-forming properties from the polynorbornene backbone and high ionic conductivity from a long-range ordered imidazolium phase. The thermal properties, morphology and ionic conductivity of the block copolymer electrolytes are investigated as a function of ionic liquid block copolymers and lithium salt contents.

2. Experimental section

2.1. Materials

6-Bromo-1-hexanol, 1-methylimidazole, ethyl vinyl ether, 5-norbornene-2-carboxylic acid (NBCOOH, 98%, mixture of endo and exo isomers), 4-dimethylaminopyridine (DMAP), lithium bis(trifluoromethanesulphonyl)imide (LiTFSI), Grubbs'

[a]School of Materials Science and Engineering, Nanchang University, 999 Xuefu Avenue, Nanchang 330031, China. E-mail: hexiaohui@ncu.edu.cn
[b]Jiangxi Provincial Key Laboratory of New Energy Chemistry, Nanchang University, 999 Xuefu Avenue, Nanchang 330031, China
[c]School of Civil Engineering and Architecture, Nanchang University, 999 Xuefu Avenue, Nanchang 330031, China

† Electronic supplementary information (ESI) available. See DOI: 10.1039/c5ra04860e

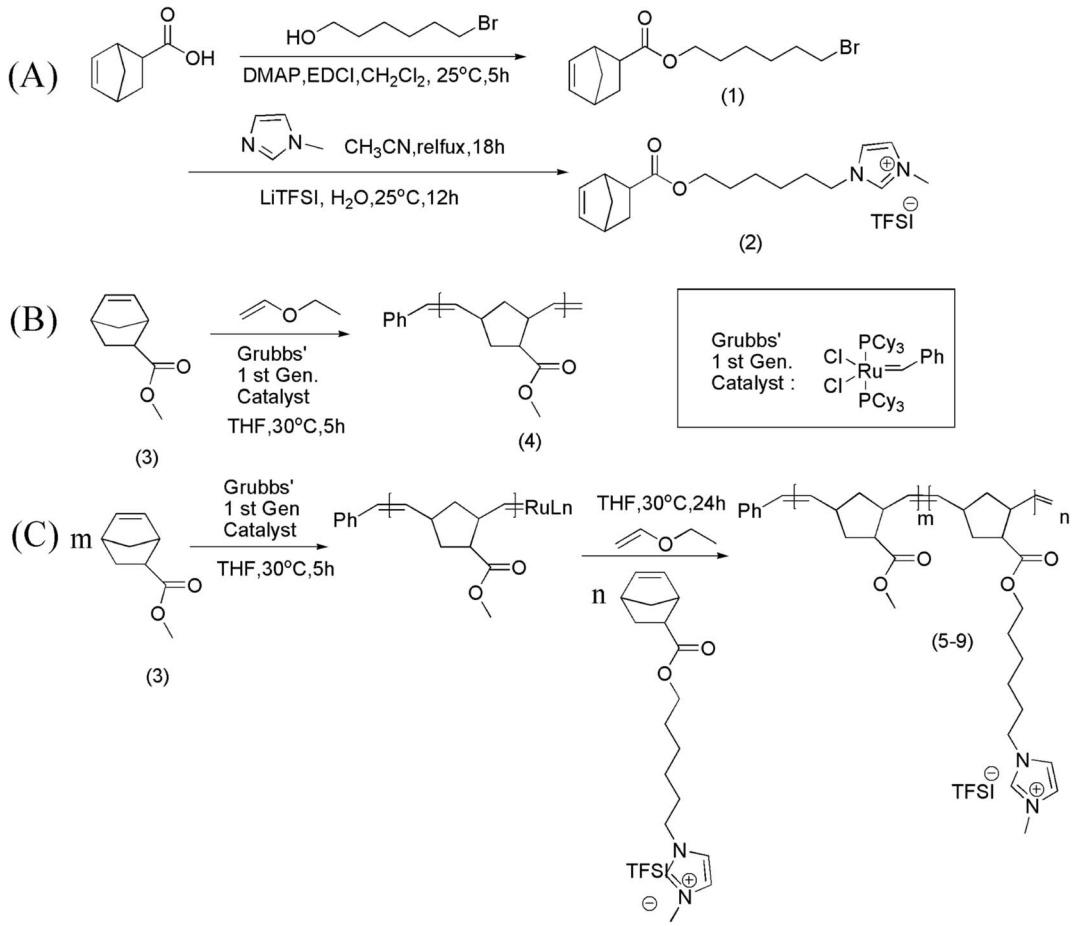

Scheme 1 Synthesis routes for monomers and copolymers.

catalyst first generation ($Cl_2(PCy_3)_2Ru$=CH-Ph), 1-(3-dimethylaminopropyl)-3-ethylcarbodiimide hydrochloride (EDCI) are used as received from Energy Chemical, methyl-5-norbornene-2-carboxylate ($NBCOOCH_3$) is purified by distillation over CaH_2 at a reduced pressure under a dry nitrogen purge just before used.

2.2. Synthesis of 5-norbornene-2-carboxylate-6-bromohexane (NBr) (1)

The synthesis of monomer is shown in Scheme 1(A). In a 100 mL round-bottomed flask equipped with a magnetic stir bar, the EDCI (8.05 g, 0.042 mol) and DMAP (catalytic amount) are added to the 30 mL CH_2Cl_2 solution of the dissolved 5-norbornene-2-carboxylic acid (4.7 g, 0.034 mol) and 6-bromo-1-hexanol (5 g, 0.028 mol). Stirring the mixture at room temperature for 5 h, then the reaction is quenched by adding water (30 mL). The crude product is extracted three times with CH_2Cl_2 and the organic layer is dried with anhydrous $MgSO_4$. Filtered, and concentrated by rotary evaporator to afford oil product. The crude mixture is further purified by column chromatography on silica gel by using hexanes/EtOAc (20 : 1) to yield a yellow oil (7.2 g, 85%). ^{1}H NMR (400 MHz, $CDCl_3$): δ = 6.15–5.90 (m, 2H), 4.05 (t, 2H), 3.50 (m, 1H), 3.36 (t, 2H), 3.16 (s, 1H), 2.99 (s, 1H), 2.85 (m, 1H), 2.13–2.22 (m, 2H), 1.92–1.79 (m, 2H), 1.68–1.21 (m, 7H).

2.3. Synthesis of 5-norbornene-2-carboxylate-1-hexyl-3-methyl-imidazolium bis((trifluoromethyl)sulfonyl)amide (NIm-TFSI) (2)

Compound **1** (6.5 g, 0.022 mol) and 1-methylimidazole (2.6 mL, 0.033 mol) are refluxing in acetonitrile for 18 h. After cooling to room temperature, the reaction mixture is concentrated under reduced pressure to afford yellow viscous oil and then washed with Et_2O (3 × 100 mL). The resulting oil is dissolved in H_2O (100 mL), LiTFSI (6.53 g, 0.023 mol) is added, and the mixture is stirred at room temperature for 12 h. The yellow oil is extracted with dichloromethane and the organic layer is washed with water and dried over anhydrous $MgSO_4$. Monomer **2** is obtained as yellow oil (10.08 g, 80%). ^{1}H NMR (400 MHz, $CDCl_3$): δ = 8.77 (s, 1H), 7.30 (d, 2H), 6.17–5.88 (m, 2H), 4.17 (t, 2H), 4.05 (t, 2H), 3.98 (m, 1H), 3.94 (s, 3H), 3.16 (s, 1H), 2.99 (s, 1H), 2.85 (m, 1H), 2.13–2.22 (m, 2H), 1.92–1.79 (m, 2H), 1.68–1.21 (m, 7H).

2.4. Synthesis of homopolymer of methyl-5-norbornene-2-carboxylate ($NB\text{-}COOCH_3$) (PMN) (4)

The synthesis of homopolymer is shown in Scheme 1(B). All polymerizations are performed under a nitrogen atmosphere, tetrahydrofuran (THF) is distilled from sodium prior to using. Grubbs' catalyst first generation [$Cl_2(PCy_3)_2Ru$=CH-Ph]

(67.0 mg, 0.08 mmol) is dissolved in 10 mL THF first, $NBCOOCH_3$ (0.609 g, 4 mmol) is added to the solution by syringe under stirring. The reaction mixture is stirred at 30 °C, after 5 h, the reaction is terminated by ethyl vinyl ether (equivalent) and continue to stir for 1 h. Then the polymer solution is precipitated in hexanes, purified, and dried under vacuum to get the brown solid.

2.5. Synthesis of ionic liquid block copolymers of methyl-5-norbornene-2-carboxylate-*block*-5-norbornene-2-carboxylate-1-hexyl-3-methyl-imidazolium bis((trifluoromethyl)sulfonyl)-amide (5–9)

The synthesis of ionic liquid block copolymers is shown in Scheme 1(C) and the typical polymerization reaction is as follows. Grubbs' catalyst (167.40 mg, 0.2 mmol) is dissolved in 10 mL THF, and then $NBCOOCH_3$ (1.272 g, 8 mmol) is added to the solution by syringe under stirring. The reaction mixture is stirred at 30 °C, and the $NBCOOCH_3$ reacted completely after 5 h, which detected by ^{1}H NMR; the monomer **2** (1.167 g, 2 mmol) is added and continue stirring for 24 h, the reaction is then terminated by ethyl vinyl ether (equivalent) and continue stirring 1 h. The polymer solution is precipitated in hexanes,[20–22] purified, and dried under vacuum to get the brown solid (1.995 g, 84%). Similar chemical shifts are observed for polymers **5–9**.

2.6. Preparation of polyelectrolyte membranes

The polyelectrolyte membranes are prepared by separately dissolving the block copolymers and lithium salt (LiTFSI) in THF for 12 h, and the mixed compositions are in four different proportions (Table 1). Then the solutions are casted on PTFE molds to prepare the polyelectrolyte films. The films are dried in the nitrogen atmosphere at room temperature for 24 h, and subsequently dried under vacuum for 48 h at 40 °C. The photograph of polyelectrolyte membrane is illustrated in Fig. 1. The films were about 150 μm thickness (Table 1).

2.7. Measurements

^{1}H NMR spectra are recorded in deuterated solvents on a Bruker ADVANCE 400 NMR Spectrometer. ^{1}H NMR chemical shifts are reported in ppm downfield from tetramethylsilane (TMS) reference using the residual protonated solvent as an internal standard. Molecular weights of the PIL block copolymers are determined by using a Waters 2410 gel permeation chromatograph (GPC) with a refractive index detector in tetrahydrofuran (THF) and using a calibration curve of polystyrene standards. Thermo gravimetric analysis (TGA) is performed on a TA-600 for thermal analysis at a heating rate of 20 °C min^{-1} under nitrogen with a sample weight of 4–10 mg. The differential scanning calorimeter (DSC, Perkin-Elmer DSC 7) is measured to determine the glass transition temperatures (T_g) of copolymers at a heating/cooling rate of 10 °C min^{-1}. The X-ray diffraction (XRD) study of the samples is carried out on a Bruker D8 Focus X-ray diffractometer operating at 30 kV and 20 mA with a copper target (λ = 1.54 Å) and at a scanning rate of 1° min^{-1}. The microphase separation studying is carried on JEOL JEM-2100F transmission electron microscope (TEM). The samples are coated on Cu grids and stained by exposing to the vapor of a 5 wt% aqueous solution of RuO_4 for 2 h to enhance contrast degree between phases before testing.[23] The ionic conductivities of polymer electrolyte membranes are performed on electrochemical impedance spectroscopy (EIS) over a frequency range of 100–1 MHz with the amplitude of 10 mV at the temperature range from 30 to 100 °C. The ionic conductivity (σ) is calculated from the following equation (eqn (1)):

$$\sigma = L/RS \quad (1)$$

where the R represents the bulk electrolyte resistance, L means the sample thickness, and S is the area of the polymer electrolyte film.

Fig. 1 The photograph of electrolyte membrane.

Table 1 Compositions and thickness of polyelectrolyte membranes

Sample (PIL mole percentage)	LiTFSI[a] (%)/thickness[b] (μm)			
21.3 mol%	5/150	—[c]	—[c]	—[c]
24.2 mol%	5/148	—[c]	—[c]	—[c]
31.0 mol%	5/150	10/146	15/152	20/150
38.7 mol%	5/148	10/152	15/150	20/148
50.7 mol%	5/150	10/154	15/150	20/148

[a] The weight ratio of LiTFSI/copolymer (wt%). [b] The thickness of electrolyte membranes. [c] The electrolyte membranes are not prepared due to the ionic conductivity is very low with the 5% LiTFSI content.

3. Results and discussion

3.1. Characterization of the monomer and polymers

The chemical structure of 5-norbornene-2-carboxylate-1-hexyl-3-methyl-imidazolium bis((trifluoromethyl)sulfonyl)amide (NIm-

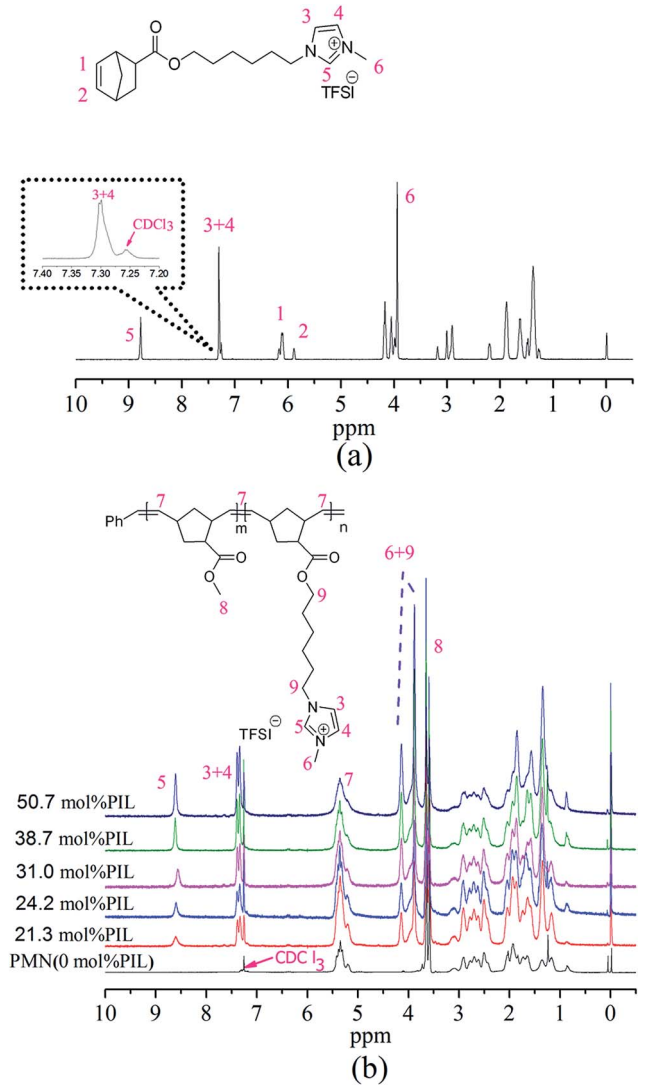

Fig. 2 ^{1}H NMR of NIm-TFSI (a) and copolymers (b).

TFSI), poly (methyl-5-norbornene-2-carboxylate) (PMN), and PIL diblock copolymers are confirmed by ^{1}H NMR spectra shown in Fig. 2. For the imidazolium-functionalized norbornene monomer, the characteristic protons absorption peaks of double bond in norbornene ring appear at 6.12 and 5.88 ppm (Fig. 2(a)). But the absorption peaks transfer to 5.50–5.13 ppm after the monomer polymerization (Fig. 2(b)). Proton absorption peaks of imidazolium ring in the monomer and ionic liquid block copolymers appear around 8.70 (CH), 7.26 to 7.33(CH=CH) and 3.92 (CH_3) are similarly. The $NBCOOCH_3$ homopolymer has no protons absorption peak between 7.26 to 8.70 ppm. And as the ionic liquid block compositions increase, the proton absorption peak areas increase gradually. The successful synthesis of the monomer and copolymers were well confirmed by the ^{1}H NMR spectra. The M_n of the copolymers obtained by GPC and Polymerized Ionic Liquids (PILs) block molar percentages are calculated[24] by ^{1}H NMR analysis. The related images are presented in the ESI (Fig. S1–S6†) and the corresponding results are exhibited in Table 2.

3.2. Thermal properties

The thermal properties of copolymers are investigated by thermogravimetry analysis (TGA) and differential scanning calorimetry (DSC). All block copolymers exhibit good thermal stability with decompositions temperatures (5% weight loss) over 390 °C (Fig. 3), which is more stable than that of the homopolymer (Table 2). The differential scanning calorimeter (DSC) curves are displayed in Fig. 4(a). All the samples are heated to 250 °C to remove thermal history first. Homopolymer has only one distinct glass transition and the PIL bock copolymers have two glass transitions that belong to the different blocks, these results indicate that the block copolymers have strong microphase-separated.[11] With the content of PIL block increases, the intensity of T_{g1} decreases, while the intensity of the T_{g2} shows the opposite tendency. Moreover, the T_gs decreases after blending with lithium salt because the large anions $TFSI^-$ has weaker association with cation,[25] and incremental content of lithium salt will further reduce the T_gs (Fig. 4(b)).

3.3. Morphology of the copolymers

The microstructure of the copolymers is studied by X-ray diffraction (XRD) (Fig. 5). All the pure copolymer films casting from their THF solutions displayed two weak diffraction peaks in the angles of ~5.6° and ~21.8°. The first reflection peak at $2\theta = 21.8°$ is the fundamental building of copolymer backbone, and the broad peaks indicate the copolymers exhibiting the amorphous structure.[26] It remains

Table 2 Molecular characteristics of copolymers

PIL diblock copolymers[a]	Feed ratio of PIL mol%	Actual ratio of PIL mol%	M_n (g mol^{-1})	PDI	T_d (°C)	T_{g1} (°C)	T_{g2} (°C)
PMN	0	0	27 874	1.04	281	—	41.39
21.3 mol%	20	21.3	33 229	1.06	385	−1.33	48.98
24.2 mol%	25	24.2	33 252	1.93	391	−3.30	48.98
31.0 mol%	33	31.0	33 502	1.04	394	−4.30	51.24
38.7 mol%	40	38.7	34 637	1.17	327	−4.98	51.24
50.7 mol%	50	50.7	37 674	2.10	400	−4.98	51.24

[a] Numbers correspond to PIL mol% that is calculated by ^{1}H NMR spectroscopy.

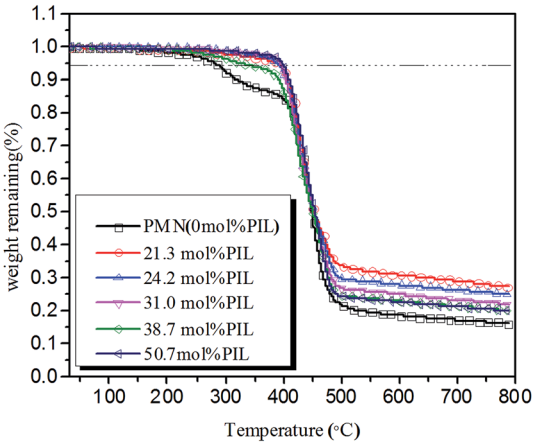

Fig. 3 TGA thermogram of PIL diblock copolymers.

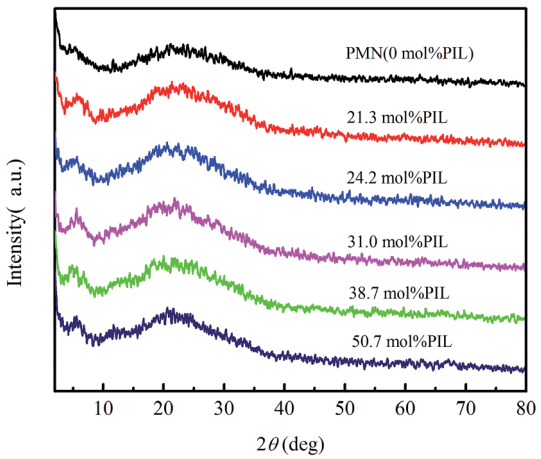

Fig. 5 XRD patterns of copolymers.

unchanged profile when the ratio of PIL composition is varied. However, the intensity of peak at $2\theta = 5.6^{\circ}$ increases along with the enhanced content of the PIL part, suggesting a more regular packing of side chain.[27,28] Transmission electron microscopy (TEM) was performed to further study the copolymers micro-morphology. The TEM images of copolymers are present in Fig. 6. The copolymers with 21.3 mol% PIL and 31.0 mol% PIL show some degree of microphase-separated morphology, but they have no long-range periodic order. While the 50.7 mol% PIL copolymer exhibits good lamella morphology with long-range periodic order clearly, this may be due to the difference electron densities between polynorbornene main chain and PIL side chains.[29] These microphase-separated morphologies are expected to provide a good passage for Li^+ transporting in the membranes.

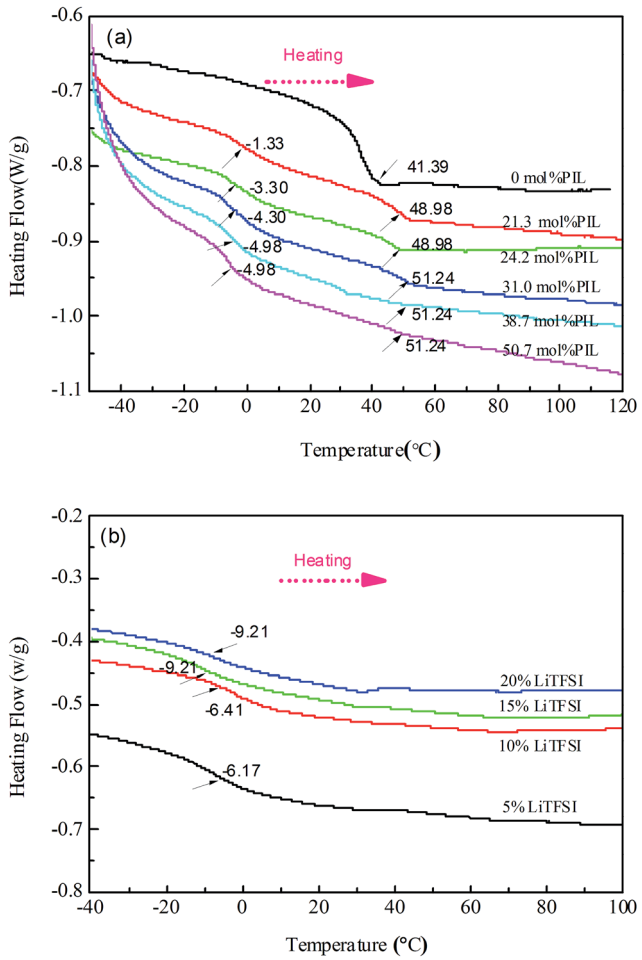

Fig. 4 DSC thermograms of copolymers (a) and polyelectrolyte of 50.7 mol% PIL with different lithium salt contents (b).

3.4. Ionic conductivity

As the homopolymer is brittle and can not form film independent, all ionic conductivities are obtained from PIL block copolymers electrolyte membranes. Fig. 7 exhibits the temperature dependence of ionic conductivity of polyelectrolyte with different PIL ratio ranging from *ca.* 21.3 to 50.7 mol% with 5% LiTFSI. Obviously, the ionic conductivity increases with the rise of temperature and PIL molar ratios. This trend may be due to the stronger segmental motion caused by high temperature, which is beneficial for ionic transport.[30,31] Besides, the PIL as the ion transporters plays an important role in improving ionic conductivity. The results show that the ionic conductivity of the polyelectrolyte with 38.7 mol% and 50.7 mol% PIL increase *ca.* 1 order of magnitude compared to the polyelectrolyte with lower PIL compositions. Fig. 8 reveals the ionic conductivity of 50.7 mol% PIL with different LiTFSI contents. The increasement of LiTFSI content can raise the concentration of Li ions, and result in enhancing the ionic conductivity. On the other hand, the block copolymer with 50.7 mol% PIL compositions exhibits good lamella morphology and it will provide a fixed ion transport channels[32] and help Li ions to transport easier and faster. The polyelectrolyte containing 50.7 mol% PIL and 20% LiTFSI offers the best ionic conductivity with 7.44×10^{-6} S cm^{-1} at 30 °C and 4.68×10^{-4} S cm^{-1} at 100 °C, respectively. However, the room conductivity achieved in our study is lower compared with the literature reported homo-PIL, and it is agree with the results that the conductivity value of solid polymer electrolytes is lower

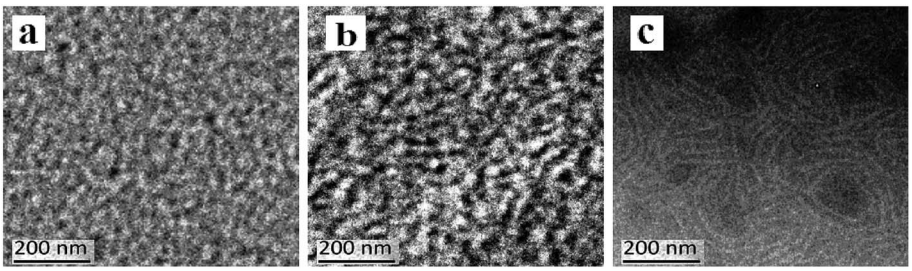

Fig. 6 TEM of copolymers: (a) 21.3 mol% PIL; (b) 31.0 mol% PIL; (c) 50.7 mol% PIL.

than that of polymer gel electrolytes.[9,10,13,33,34] On the other side, like the other similarity PIL block copolymers,[11,12,35] these copolymers do not apply to lithium ion battery.

The ionic conductivities of other copolymer electrolytes with different lithium salt contents are also measured (Table 3). As expected, the ionic conductivities increase with the enhancement of PIL compositions and LiTFSI contents.

Because the cation is fixed on the polymer chain and only the anion is mobile, PIL block copolymer electrolyte is single-ion conductor. Therefore, the connectivity of conducting (*i.e.*, ions ion-to-ion hopping distance) has significant impact on ion transport.[11] In the PIL block units, the high concentration of ion conductors is helpful for shorting the anion-to-anion hopping distance, and leading to low hopping energy and the efficiency of ion transport. Consequently, the increased PIL compositions made the local concentration of conducting ions up-shift and thus enhanced the ionic conductivity.

From Fig. 7 and 8, It can be found that the ionic conductivity approximately linear increases with the temperature increasing, which obeys the Arrhenius equation (eqn (2)):

$$\sigma(T) = A \exp\left(\frac{-E_a}{RT}\right) \quad (2)$$

where σ is the ionic conductivity, A is the pre-exponential factor, E_a is the activation energy of ion conduction, and R is the gas constant and T is the absolute temperature. E_a is calculated from the slope of the fitting lines with the temperature range of 373–303 K. The calculated E_a values are 27.56 kJ mol^{-1} (50.7 mol% PIL/5% LiTFSI polyelectrolyte membrane), 26.77 kJ mol^{-1} (50.7 mol% PIL/10% LiTFSI polyelectrolyte membrane), 24.78 kJ mol^{-1} (50.7 mol% PIL/15% LiTFSI polyelectrolyte membrane) and 24.39 kJ mol^{-1} (50.7 mol% PIL/20% LiTFSI polyelectrolyte membrane), respectively. The E_a values of polyelectrolyte membranes have a small change, and it agrees with that the lower activation energy getting the higher ionic conductivity.[36]

3.5. Electrochemical stability

Electrochemical stability window of the polyelectrolyte is characterized by linear sweep voltammetry using the cell SS|polymer electrolyte|Li. In the measurement, we choose two typicality high ionic conductivity polyelectrolytes, and the results are shown in Fig. 9. Both of polyelectrolytes exhibit suitable electrochemical stability. Although the polyelectrolyte with PIL ratio of 31.0 mol% is relatively more stable due to the less content of ionic liquids. The polyelectrolyte of 50.7 mol% PIL compositions decomposed at about 4.2 V *versus* Li/Li$^+$ at 30 °C, demonstrating it can be applied to lithium ion batteries.

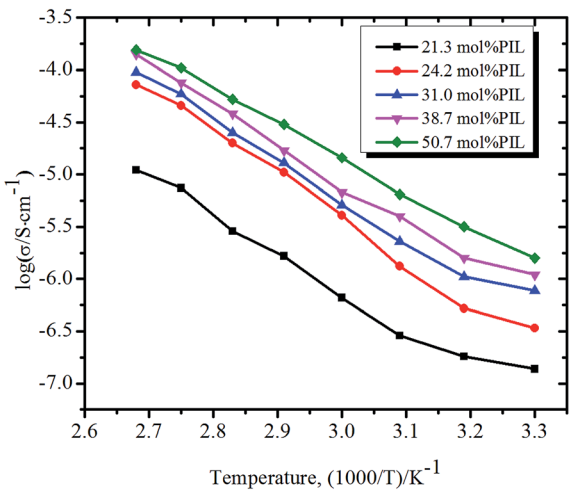

Fig. 7 Temperature dependence of ionic conductivity of polyelectrolyte with 5% LiTFSI.

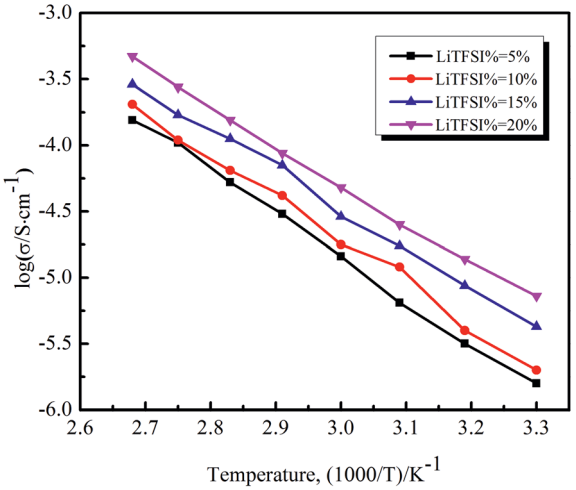

Fig. 8 Temperature dependence of ionic conductivity of polyelectrolyte of 50.7 mol% PIL with various LiTFSI components.

Table 3 Ionic Conductivity of polyelectrolyte with different lithium salt contents

	Conductivity ($\times 10^{-6}$ S cm^{-1})							
Copolymer electrolytes	LiTFSI (5%)		LiTFSI (10%)		LiTFSI (15%)		LiTFSI (20%)	
Temperature/°C	30	100	30	100	30	100	30	100
50.7 mol%	1.58	156	2.02	201	4.27	289	7.44	468
38.7 mol%	1.09	154	1.55	184	3.97	239	7.18	272
31.0 mol%	0.78	94	1.33	137	2.51	169	3.97	203

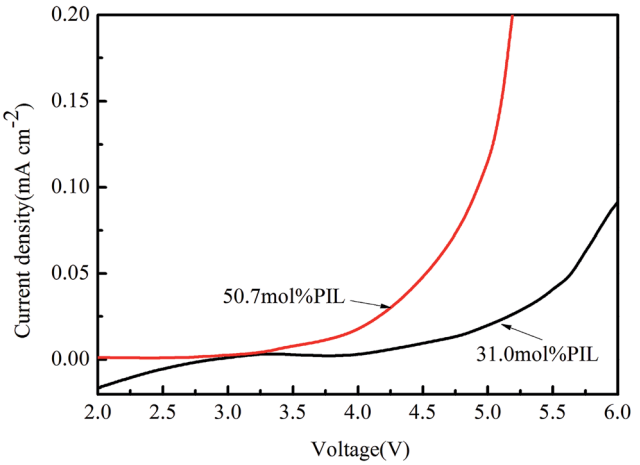

Fig. 9 Linear sweep voltammetry curves of the cells prepared for electrolytes with 20% LiTFSI (1 mV s^{-1}, SS: stainless steel).

4. Conclusion

In this study, we synthesized a series of ionic liquid block copolymers *via* ring-opening metathesis polymerization, and the copolymers show good thermal stability and the obvious two glass transition temperatures that indicating the strong microphase separation. Especially, the 50.7 mol% PIL copolymer exhibits good lamella morphology with long-range periodic order clearly in TEM image. In this system of polyelectrolyte, the higher PIL block compositions as well as lithium salt contents are beneficial for ionic conductivity. The polyelectrolyte with 50.7 mol% PIL compositions and 20% LiTFSI offers the best ionic conductivities with 7.44×10^{-6} S cm^{-1} at 30 °C and 4.68×10^{-4} S cm^{-1} at 100 °C, and the values are largely improved compared to other low PIL compositions block polymers. Moreover, the polyelectrolyte also exhibits good electrochemical stability and decomposes at about 4.2 V *versus* Li/Li^{+}. Considering that the good corresponding properties of the block copolymers, such as stability and ionic conductivity, they will be one of the potential candidate materials for lithium ion battery.

Acknowledgements

This work is supported by the National Natural Science Foundation of China (51463014 and 21164006).

References

1 C. F. Yuan, J. Li, P. F. Han, Y. Q. Lai, Z. A. Zhang and J. Liu, *J. Power Sources*, 2013, **240**, 653–658.
2 Y. Wang, B. Li, J. Y. Ji and W. H. Zhong, *J. Power Sources*, 2014, **247**, 452–459.
3 Q. W. Lu, J. H. Fang, J. Yang, G. W. Yan, S. S. Liu and J. L. Wang, *J. Membr. Sci.*, 2013, **425**, 105–112.
4 X. Zuo, X. M. Liu, F. Cai, H. Yang, X. D. Shen and G. Liu, *J. Power Sources*, 2013, **239**, 111–121.
5 D. F. Miranda, C. Versek, M. T. Tuominen, T. P. Russell and J. J. Watkins, *Macromolecules*, 2013, **46**, 9313–9323.
6 J. Y. Yuan and M. Antonietti, *Polymer*, 2011, **52**, 1469–1482.
7 J. M. Lu, F. Yan and J. Texter, *Prog. Polym. Sci.*, 2009, **34**, 431–448.
8 M. Armand, F. Endres, D. R. MacFarlane, H. Ohno and B. Scrosati, *Nat. Mater.*, 2009, **8**, 621–629.
9 M. T. Li, B. L. Yang, L. Wang, Y. Zhang, Z. Zhang, S. H. Fang and Z. X. Zhang, *J. Membr. Sci.*, 2013, **447**, 222–227.
10 M. T. Li, L. Wang, B. L. Yang, T. T. Du and Y. Zhang, *Electrochim. Acta*, 2014, **123**, 296–302.
11 Y. S. Ye, J. H. Choi, K. I. Winey and Y. A. Elabd, *Macromolecules*, 2012, **45**, 7027–7035.
12 J. H. Choi, Y. S. Ye, Y. A. Elabd and K. I. Winey, *Macromolecule*, 2013, **46**, 5290–5300.
13 K. Yin, Z. X. Zhang, L. Yang and S. I. Hirano, *J. Power Sources*, 2014, **258**, 150–154.
14 M. D. Green, J. H. Choi, K. I. Winey and T. E. Long, *Macromolecules*, 2012, **45**, 4749–4757.
15 Y. Schneider, M. A. Modestino, B. L. McCulloch, M. L. Hoarfrost, R. W. Hess and R. A. Segalman, *Macromolecules*, 2013, **46**, 1543–1548.
16 M. Lee, U. H. Choi, R. H. Colby and H. W. Gibson, *Chem. Mater.*, 2010, **22**, 5814–5822.
17 M. Döbbelin, I. Azcune, M. Bedu, A. R. Luzuriaga, A. Genua, V. Jovanovski, G. Cabañero and I. Odriozola, *Chem. Mater.*, 2012, **24**, 1583–1590.
18 M. T. Li, L. Yang, S. H. Fang, S. M. Dong, S. Hirano and K. Tachibana, *J. Power Sources*, 2011, **196**, 8662–8668.
19 M. T. Li, L. Yang, S. H. Fang, S. M. Dong, S. Hirano and K. Tachibana, *Polym. Int.*, 2012, **61**, 259–264.
20 S. Biswas, K. D. Belfield, R. K. Das, S. Ghosh and A. F. Hebard, *Chem. Mater.*, 2009, **21**, 5644–5653.
21 H. R. Allcock, J. D. Bender, R. V. Morford and E. B. Berda, *Macromolecules*, 2003, **36**, 3563–3569.
22 M. R. Xie, J. Y. Dang, J. X. Shi, H. J. Han, C. M. Song, W. Huang and Y. Q. Zhang, *Acta Chim. Sin.*, 2009, **67**, 869.
23 R. L. Weber, Y. S. Ye, A. L. Schmitt, S. M. Banik, Y. A. Elabd and M. K. Mahanthappa, *Macromolecules*, 2011, **44**, 5727–5735.
24 E. F. Wiesenauer, J. P. Edwards, V. F. Scalfani, T. S. Bailey and D. L. Gin, *Macromolecules*, 2011, **44**, 5075–5078.
25 H. Chen, J. H. Choi, D. S. Cruz, K. I. Winey and Y. A. Elabd, *Macromolecules*, 2009, **42**, 4809–4816.
26 W. S. Chi, S. U. Hong, B. Jung, S. W. Kang, Y. S. Kang and J. H. Kim, *J. Membr. Sci.*, 2013, **443**, 54–61.

27 N. Leventis, C. S. Leventis, D. P. Mohite, Z. J. Larimore, J. T. Mang, G. Churu and H. B. Lu, *Chem. Mater.*, 2011, **23**, 2250–2261.
28 S. Ahn, P. Deshmukh and R. M. Kasi, *Macromolecules*, 2010, **43**, 7330–7340.
29 S. H. Yeon, S. H. Ahn, J. H. Kim, K. B. Lee, Y. Jeong and S. U. Hong, *Polym. Adv. Technol.*, 2012, **23**, 516–521.
30 M. A. Ratner, *in Polymer Electrolyte Reviews-1*, ed. J. R. MacCallum and C. A. Vincent, Elsevier Science Publishing Co., Inc., New York, 1987, p. 173.
31 M. Armand, *Solid State Ionics*, 1983, **9–10**, 745–754.
32 Y. F. Zhang, C. A. Lim, W. W. Cai, R. Rohan, G. D. Xu, Y. B. Sun and H. S. Cheng, *RSC Adv.*, 2014, **4**, 43857–43864.
33 I. Stepniak, E. Andrzejewska, A. Dembna and M. Galinski, *Electrochim. Acta*, 2014, **121**, 27–33.
34 F. Cai, X. Zuo, X. M. Liu, L. Wang, W. Zhai and H. Yang, *Electrochim. Acta*, 2013, **106**, 209–214.
35 J. R. Nykaza, Y. S. Ye and Y. A. Elabd, *Polymer*, 2014, **55**, 3360–3369.
36 W. Xiao, C. Miao, X. Q. Yin, Y. C. Zheng, M. L. Tian, H. Li and P. Mei, *J. Power Sources*, 2014, **252**, 14–20.